Lagrangian descriptor and escape time as tools to investigate the dynamics of laser-driven polar molecules

M. D. Forlevesi [1,*] R. Egydio de Carvalho [1,†] and Emanuel F. de Lima [2,‡]

[1] *Universidade Estadual Paulista–UNESP, Instituto de Geociências e Ciências Exatas–IGCE, Departamento de Estatística, Matemática Aplicada e Ciências da Computação, Rio Claro-SP 13506-900, Brazil*

[2] *Departamento de Física, Universidade Federal de São Carlos, São Carlos-SP 13565-905, Brazil*

(Received 11 November 2022; revised 25 January 2023; accepted 3 February 2023; published 17 February 2023)

We consider the nonlinear dynamics of a diatomic polar molecule under a linearly polarized laser field. We assume a model in which the molecule dipole is coupled with a time-dependent electric field. This system presents a bound energy region where the atoms are bound, and a free-energy region where the atoms are dissociated. Due to the nonalignment between the dipole axis and the laser direction, and the time dependence of the external field, this system presents two and a half degrees of freedom, namely the vibrational degree, the rotation degree, and the time. To investigate the system dynamics, instead of using the Poincaré surface-of-section technique, we propose the use of the Lagrangian descriptor associated with the escape times. The Lagrangian descriptor is a quantity that reveals complex structures in the phase space, whereas the escape times are the time span in which a trajectory is initially in the bound region before escaping to the unbound region. The combination of these two quantities allows us to distinguish between real stability regions from other complex structures, including stickiness regions, and a different formation, which we call escape islands. With the help of these tools, we find that for high-field amplitudes the inclusion of rotation leads to an increase of the stability regions, which implies a decrease of the dissociation in comparison with the one-dimensional case.

DOI: 10.1103/PhysRevE.107.024209

I. INTRODUCTION

A very important task in physics, with a vast number of applications, is the investigation of the dynamics of atoms and molecules under the action of time-dependent external fields. The classical approaches have several motivations, including finding quantum-classical correspondence allowing for a useful nonlinear-dynamics interpretation; understanding the influence of nonlinear forces on particle dynamics; the possibility of controlling chaotic dynamics [1,2]; applications to molecular process [3]; and laser control chemistry [4].

In this work, we investigate the nonlinear classical dynamics of a polar molecule under the influence of a linearly polarized laser field. We consider the driven rotational forced Morse potential [5] as a model for the study of the interaction between the external field of the laser with the diatomic molecule, considering the angular momentum of the molecule, and the polarization angle between the applied laser and the molecular dipole moment. This is a two-and-a-half degrees of freedom system. The driven Morse oscillator is an important model for studying the classical and quantum behavior of diatomic molecules [5–12]. The unperturbed Morse oscillator presents two distinct types of motion: libration, which corresponds to a bound vibrating molecule, and unbound motion, which corresponds to a free or colliding atomic pair. The threshold energy that separates the two kinds of motion defines the separatrix in the phase space. The coupling between the molecular dipole and a time-dependent external field, produced by a laser, can induce changes in the dynamics of the system. For null external field, the phase space is filled by invariant tori and periodic orbits. As the amplitude of the external field increases, resonance islands, chaotic orbits, and periodic orbits can coexist [6].

The simplest autonomous systems that can exhibit chaos are those with two degrees of freedom whose phase space has four dimensions, and the Poincaré section (PS) technique is a frequent tool to analyze the dynamics. For a system with more degrees of freedom, this technique is not useful for understanding the dynamics. To get around this problem, several methods have been developed to study the dynamics of high-dimensional systems [13]. Among them, a tool known as a Lagrangian descriptor (LD), which focuses on the structures of the phase space that are immersed in the chaotic region, was introduced in Ref. [14] to study nonperiodic flows. It was also applied in other systems such as maps [15], stochastic systems [16], and in the identification of reactive islands responsible for nonstatistical behavior in chemical reactions [17], among others [18–24].

In the current work, we will apply the LD, associated with the escape time (ET) technique, which represents the time that an initial condition confined in the well takes to escape the influence of the potential, to study and understand a system with two and a half degrees of freedom. The PS will also be useful to calibrate the ET when photoassociation or photodissociation occur in a system without rotation and with one and a half degrees of freedom. Next, the LD will be used to visualize the dynamics, in place of the PS, for the forced rotational Morse potential, which has one more

*forlevesi@gmail.com
†ricardo.egydio@unesp.br
‡emanuel@df.ufscar.br

degree of freedom. The combination of both techniques will allow us to identify chaotic dynamics, stability islands, and stickiness regions. These regions form archipelagos of small islands of stability coming from the destruction of invariant tori, and they provide a temporary confinement of orbits in their areas. Stickiness, in general, occurs in the neighborhood of greater stability islands, but it can also occur in small regions immersed in the sea of chaos.

The paper is organized as follows: in Sec. II we present the model under consideration, in Sec. III we introduce the LD and ET techniques, in Sec. IV we present the results, and in Sec. V we provide the final remarks and the conclusions.

II. THE MODEL

We consider the relative motion of a pair of colliding atoms in the presence of a linearly polarized laser field. A suitable unperturbed dimensionless Hamiltonian for describing the relative motion of the nuclei of a diatomic molecule with rotation is given by [25,26]

$$H(x,\, p_x,\, p_\theta) = \frac{p_x^2}{2} + \frac{1}{2}\frac{p_\theta^2}{(x+x_e)^2} + V(x) \tag{1}$$

with

$$V(x) = \tfrac{1}{2}(e^{-2x} - 2e^{-x}) \tag{2}$$

in which x is the distance between the nuclei, p_x is its conjugate linear momentum, and p_θ is the conjugate angular momentum of the nuclei relative motion. $V(x)$ is the Morse potential. The energy of the bottom of the well is -0.5, and the energy of the separatrix is given by $V(x) = 0$. So, for negative energies the trajectories are bounded, representing a vibrating molecule, and for positive energies the trajectories are unbounded, representing free atomic pairs.

The laser-molecule interaction is described in the dipole approximation by the term

$$V_{\text{laser}}(x,\eta,\theta,t) = -\mu(x,\eta)\varepsilon(t)\cos(\theta), \tag{3}$$

where $\varepsilon(t)$ is the time-dependent electric laser field, $\mu(x,\eta)$ is the dipole moment of the molecule that is going to be formed, and θ is the polarization angle. We use a functional form for the dipole moment, which allows us to control its shape and its range through adjustable parameters [31], given by

$$\mu(x,\eta) = e^{-\xi\,(x+x_e)^4}\,\frac{\sin[\,\eta\,(x+x_e)\,]}{\eta}, \tag{4}$$

with η, x_e, and ξ being the dimensionless adjustable parameters.

Depending on the choice of parameters, the dipole function given in Eq. (4) allows us to reproduce realistic dipole functions [27–30]. The parameter η controls its oscillatory behavior, the parameter ξ sets its range, while x_e gives the overall displacement of the dipole. In addition, it has been shown that the oscillatory behavior of the dipole function can prevent trajectories from escaping the potential well, influencing the dynamics of the system [31].

The external electric laser field is written as

$$\varepsilon(t) = \varepsilon_0 \sin(\Omega t), \tag{5}$$

where ε_0 and Ω are the amplitude and frequency of the laser, respectively.

Hence, the model with two and a half degrees of freedom that we are considering has the total Hamiltonian given by

$$\begin{aligned} H(x,\, p_x,\, \theta,\, p_\theta,\, t) &= \frac{p_x^2}{2} + \frac{1}{2}\frac{p_\theta^2}{(x+x_e)^2} + \frac{1}{2}(e^{-2x} - 2e^{-x}) \\ &\quad - \varepsilon_0\, \sin(\Omega t)\, e^{-\xi\,(x+x_e)^4}\,\frac{\sin[\,\eta\,(x+x_e)\,]}{\eta}\cos(\theta) \end{aligned} \tag{6}$$

and the corresponding equations of motion are

$$\frac{dx}{dt} = p_x, \tag{7a}$$

$$\begin{aligned} \frac{dp_x}{dt} &= \frac{p_\theta^2}{(x+x_e)^3} + (e^{-2.x} - e^{-x}) \\ &\quad + \varepsilon_0\, \sin(\Omega t)\frac{e^{-\xi(x+x_e)^4}}{\eta}[\eta\, \cos[\eta\,(x+x_e)] \\ &\quad - 4\,\xi\,(x+x_e)^3][\sin[\eta\,(x+x_e)]\,]\cos(\theta), \end{aligned} \tag{7b}$$

$$\frac{d\theta}{dt} = \frac{p_\theta}{(x+x_e)^2}, \tag{7c}$$

$$\frac{dp_\theta}{dt} = -\varepsilon_0 \sin(\Omega t)\, e^{-\xi\,(x+x_e)^4}\,\frac{\sin[\,\eta\,(x+x_e)\,]}{\eta}\,\sin(\theta). \tag{7d}$$

The equations above generate the entire dynamics of the system. Note that if $p_\theta = 0$, if the variable θ is constant, and if we have only two time-dependent equations of motion associated with the one-and-a-half degrees of freedom case, it is possible to use the stroboscopic PS to visualize the structures present in the phase space $(x,\, p_x)$. On the other hand, if $p_\theta \neq 0$, the angle θ is no longer constant and the system has two and a half degrees of freedom, so that we need other tools to study the dynamics.

III. LAGRANGIAN DESCRIPTOR AND THE ESCAPE TIME

To understand the dynamics of the rotational case, we will start with the nonrotational case and use the PS for the configurations of interest with the objective of calibrating the results from the LD, which can reveal the structures that are hidden in the chaotic regions of the system. Next, the ET will be used to distinguish the regular structures of the chaotic regions and identify the regions of stickiness.

The PS, for the 1.5 degrees of freedom, is constructed as follows: a grid of initial conditions is given and evolved in time. Whenever the oscillatory term of the electric field is null, that is, when $t = (2n\pi/\Omega)$, $n = 0,\, 1,\, 2\ldots$, we collect the x and p_x generating the PS for the established set of parameters.

The LD measured is based on the computation of an arc length of a trajectory, and it is extended along the trajectories by considering the integration of the velocity field for an interval of time. We use the definition proposed in [32–35], which allows us to identify the structures of the phase space

with little computational effort. We introduce the definition of the LD as

$$M_p(z_0,\,\tau) = \int_{-\tau}^{\tau} (|\dot{x}|^p + |\dot{p}_x|^p + |\dot{\theta}|^p + |\dot{p}_\theta|^p)dt. \quad (8)$$

To construct the LD, we integrate the equations of motion through a fourth-order Runge-Kutta method with a fixed step, $h = 10$–6. This value was defined after several convergence tests for each initial condition and for a long integration time. For each iteration, we calculate $(x,\, p_x,\, \theta,\, p_\theta,)$ and substitute them in Eqs. (7a)–(7d), thus obtaining the velocity field $(\dot{x},\ \dot{p}_x,\ \dot{\theta},\ \dot{p}_\theta)$. Next, we have the value of LD computing the integral in Eq. (8). This process is repeated for a grid of initial conditions. The color map is a projection of the LD in the plane $(x,\, p_x)$. Note that the most important issue is not to analyze the absolute values of the LD but the change of their values (their colors).

It is important to emphasize that the integration time τ and the parameter p play important roles in the calculation of the LD. It was shown, in a recent study [35], that these parameters are associated with the quantity of structures revealed in the dynamics. The ideal value of τ and the norm p are found through trial and error.

Finally, we calculate the ET from the initial conditions of the system. We evolve each trajectory with initial negative energy over time, and when this trajectory reaches a positive energy, positioned such that $x > 5$ and $p_x > 0$, we say that it escapes the action of the potential well. When this occurs, we define this time as being the T_E.

IV. RESULTS AND DISCUSSION

In this section, we apply the techniques proposed in the previous section to the system with two and a half degrees of freedom, and we show that they are effective for studying the changes that occur in the dynamics with the introduction of rotation. For that, we first present the PS, the LD, and the ET for the one-and-a-half-dimensional system.

Throughout this study, we will use the following values for the parameters of the dipole moment: $\eta = 1$, $\xi = 1$, and $x_e = 1$, while for the electric field we will consider two different amplitudes—$\varepsilon_0 = 0.0805$ and 0.50—and a fixed frequency $\omega = \sqrt{3}$. Finally, the parameters of the LD are $p = 0.4$ and $\tau = 10^5$. These parameters were chosen to allow a better visualization of the maps.

To generate the PS for the nonrotating system, we consider the following grid of initial conditions $x_0 = [-1 : 2.5]$ and $px_0 = [-1.0 : 1.0]$ with steps 0.1 for both variables. To build the LD and ET, we consider $x_0 = [-1 : 2.5]$, $\Delta x_0 = 0.05$, $px_0 = [-1.0 : 1.0]$, and $\Delta px_0 = 0.05$.

Figure 1(a) shows the PS, in which we can see a resonance island centered at the equilibrium point $(x,\ p_x) = (0, 0)$ and two other islands, immersed in a chaotic sea. Figure 1(b) presents the corresponding LD, where we can observe the same islands and the chaotic regions shown in Fig. 1(a). We also observe some new structures that are not present in the PS, such as the structures located between $x \sim [-0.5 : 0]$ and $p_x \sim [-0.75 : -0.4]$ and between $x \sim [0.9 : 1.5]$ and $p_x \sim [-0.1 : 0.5]$. Figure 1(c) shows the ET for each initial condition. The black color corresponds to long ET, and therefore

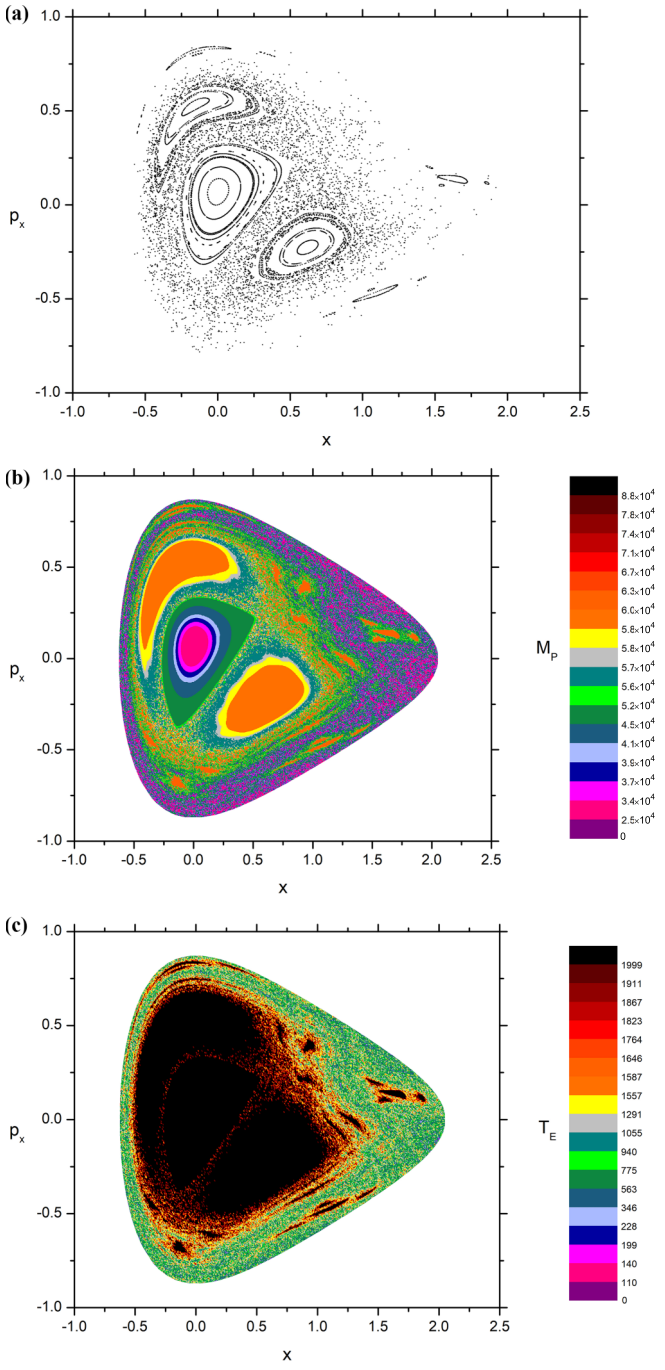

FIG. 1. For the nonrotating system, we show (a) a Poincaré section, (b) a Lagrangian descriptor, and (c) escape time. The parameters are $E_0 = -0.12$, $\varepsilon_0 = 0.0805$, $\omega = \sqrt{3}$, $\eta = 1$, $\xi = 1$, and $x_e = 1$.

the initials conditions in these regions do not escape from the influence of the potential well. Note that the additional structures revealed by the LD correspond to the islands of resonance. Furthermore, Fig. 1(c) shows that around all the islands the orbits will be trapped for a long time before escaping due to the stickiness. For instance, around the islands at $x \sim [1.4 : 1.8]$ and $px \sim [0 : 0.25]$ the orbits in their neighborhood have high ET, in the interval $TE \sim [1823 : 1999]$, indicating the action of the stickiness.

Now, we introduce rotation so that the system is described by two and a half degrees of freedom, represented by the

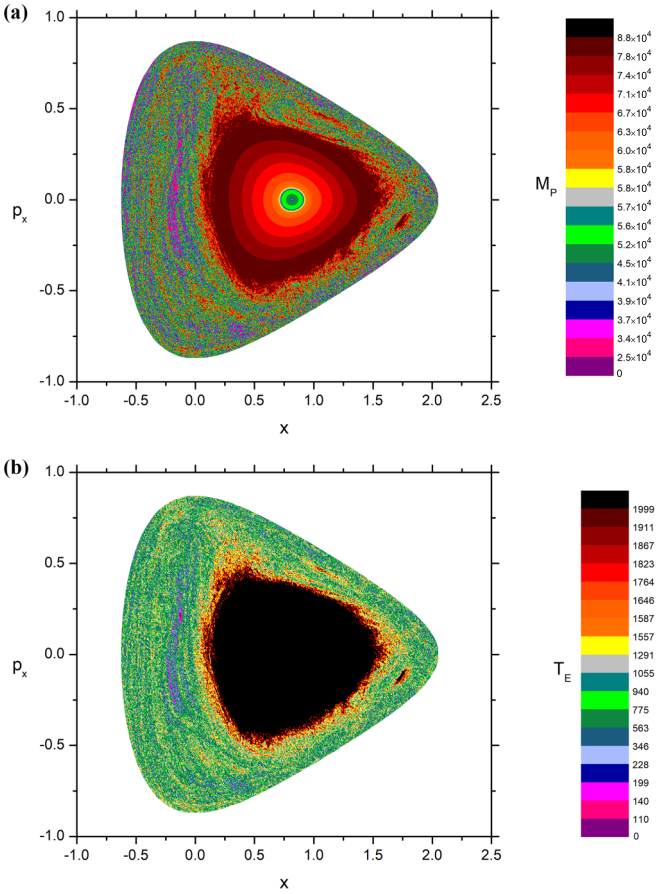

FIG. 2. For the rotational system, we show in (a) a Lagrangian descriptor and (b) escape time. The parameters are $E_0 = -0.12$, $\varepsilon_0 = 0.0805$, $\omega = \sqrt{3}$, $\eta = 1$, $\xi = 1$, and $x_e = 1$.

relative position of the atoms and their conjugate linear momentum, the angle between the electric field and the molecular dipole and their conjugate angular momentum, and time. In this scenario, the PS technique becomes inadequate because the dynamics is four-dimensional and the projections in the planes of phase present crossings of tori. So, we study the influence of the rotation by using the LD and the ET. We compose both of these techniques because the LD alone is not able to distinguish real islands of stability from other complex islandlike structures. To construct the LD and the ET for the rotational system, we consider the same initial conditions—$x_0 = [-1 : 2.5]$, $\Delta x_0 = 0.05$, $px_0 = [-1.0 : 1.0]$, and $\Delta px_0 = 0.05$—assuming that all orbits have the initial energy $E_0 = -0.12$. The value of the initial angle is $\theta_0 = \pi$, and the conjugate angular momentum is found from

$$p_{\theta 0} = (x_0 + x_e)\sqrt{2E_0 - p_{x0}^2 - (e^{-2x_0} - e^{-x_0})}. \quad (9)$$

Figures 2(a) and 2(b) show that the addition of the rotation changes the number and the position of the equilibrium points of the system. In contrast to the three resonance islands seen in the nonrotating case, now a single region of stability is perceived. Note that Fig. 2(b) shows that this region has infinite ET (indicated in black). On the other hand, it is also possible to see that the initial conditions around this region, and the other resonance islands, have high ET,

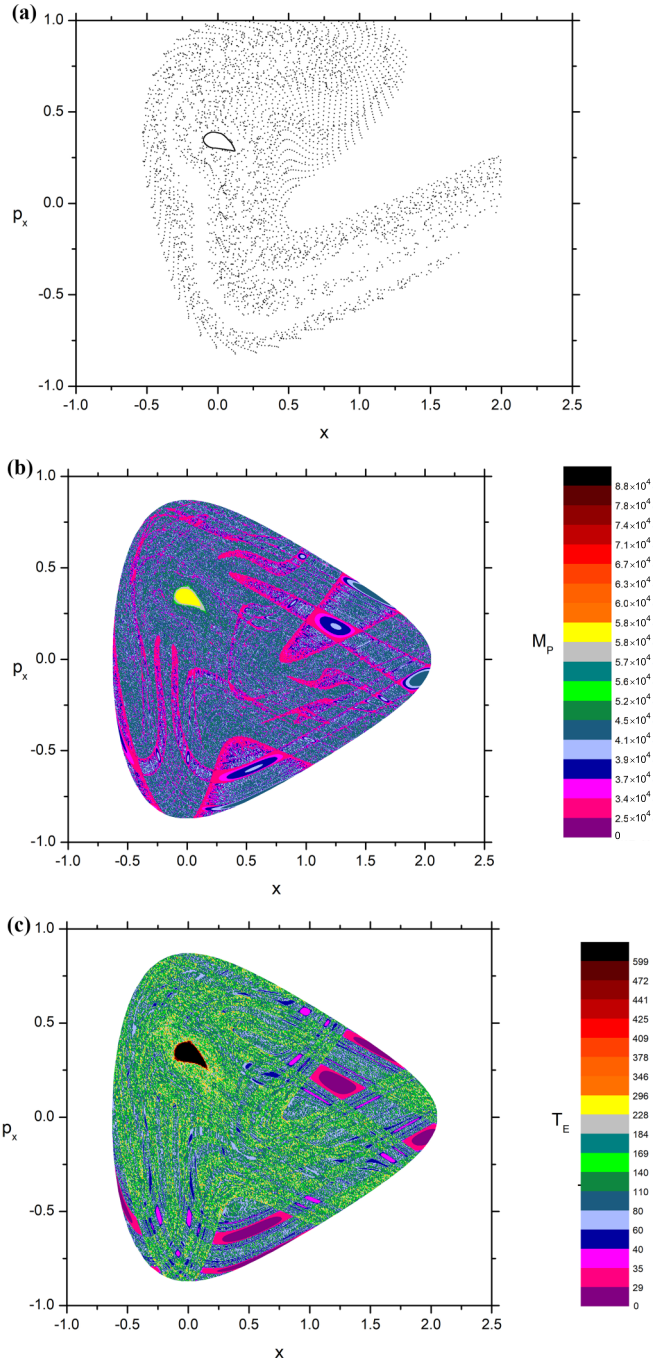

FIG. 3. For the nonrotating system, we show (a) a Poincaré section, (b) a Lagrangian descriptor, and (c) escape time. The parameters are $E_0 = -0.12$, $\varepsilon_0 = 0.50$, $\omega = \sqrt{3}$, $\eta = 1$, $\xi = 1$, and $x_e = 1$.

$T_E \sim [1764 : 1999]$, which characterizes again the stickiness in the system. Therefore, we can conclude that for the set of parameters used, the nonlinear dynamics techniques allowed us to study the dynamics of the system and to identify the possibilities of photoassociation and photodissociation even for the 2.5-degrees-of-freedom case. Stable and unstable structures as well as stickiness are revealed in the system.

We now repeat this study for the same parameters but for a higher electric field amplitude, $\varepsilon_0 = 0.50$. For the case without rotation, in Fig. 3(a), which shows the PS, we can see that

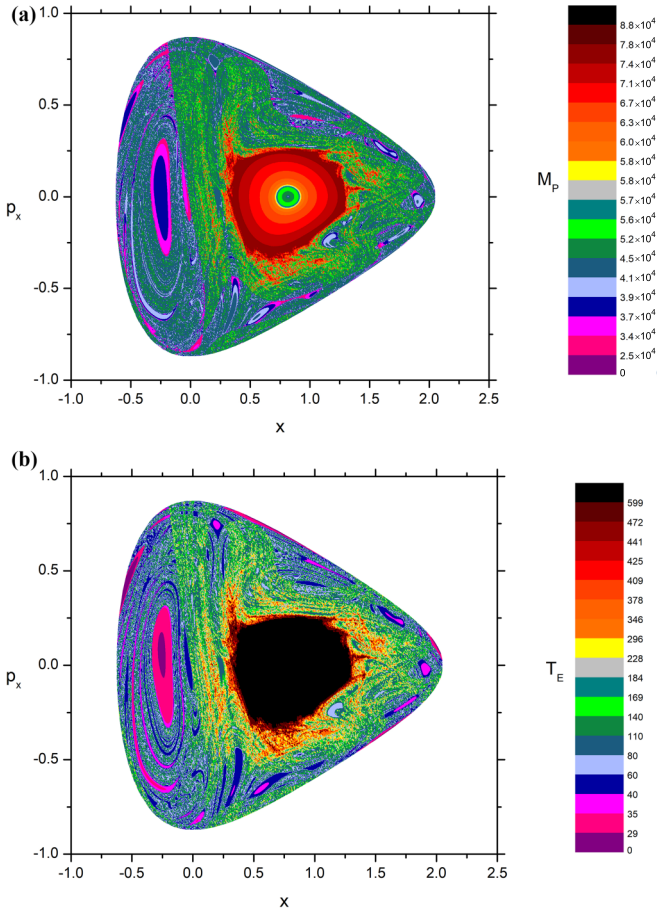

FIG. 4. For the rotational system, we show (a) a Lagrangian descriptor and (b) escape time. The parameters are $E_0 = –0.12$, $\varepsilon_0 = 0.50$, $\omega = \sqrt{3}$, $\eta = 1$, $\xi = 1$, and $x_e = 1$.

there is only a small island of stability around the equilibrium point, the rest of the dynamics being represented by chaos. On the other hand, the LD shows that some islands exist that seem to be stable, such as the one in $x = [0.25 : 0.75]$ and $p_x = [–0.7 : –0.5]$, and $x = [1.1 : 1.5]$ and $p_x = [0.1 : 0.3]$, but Fig. 3(c) shows that the trajectories that are in these structures have ETs of $T_E < 29$. These regions have a shorter ET than the trajectories that are in their chaotic neighborhoods. Furthermore, the only trajectories that do not escape from the potential are those in black that are close to the equilibrium point, whose neighborhood presents stickiness. In the next figures, we present the LD and ETs for the system with rotation.

Figure 4(a) shows that when rotation is introduced with a high amplitude, the stable region (the region with infinite escape time) increases considerably, that is, for this case the rotation avoids the initial conditions to reach positive energy and $x > 5$. Furthermore, we see that the initial conditions in these regions have escape times between $T_E \sim [425 : 599]$, showing stickiness around the equilibrium point. Due to this increasing of the stable region, we note that the introduction of rotation should decrease the photodissociation probability. Finally, comparing Fig. 3(c) with Fig. 4(b) we see that there are regions shown by a predominantly pink color, i.e., with small ET taking islandlike shapes, which could be confused with islands of stability. We call such islands structures "*escape islands.*" Note that these structures are only present in a high-amplitude electric field regime.

In performing a qualitative analysis for the results of the LD and the ET, we verified that within the escape islands there is, in principle, an inversely proportional behavior between them, that is, when one increases the other decreases. For instance, consider the escape island in Figs. 4(a) and 4(b) located at $x \sim [–0.5 : 0]$ and $p_x \sim [–0.4 : 0.4]$. Figure 4(a) shows that the values of the LD of the inner island (blue) are greater than those of the LD of the outer island (light pink). On the other hand, Fig. 4(b) shows that the inner island (purple) has a smaller ET compared to the outer island (pink). This relationship between the LD and the ET can be observed in all escape islands. However, this observation does not seem to be true for other regions. In fact, we observe that the stable region centered at $x \sim 0.75$ and $p_x \sim 0$ in Fig. 4(b), which has the largest values of ET in this plot, corresponds to the largest values of the LD in Fig. 4(a). This rather complex correlation will be investigated in future work.

V. CONCLUSION

In this work, we study the dynamics of a polar molecule under a linearly polarized laser field. The problem is modeled by the driven Morse oscillator with rotation. Since it is not possible to obtain the PS for systems with two and a half degrees of freedom, we analyze the system through the application of two complementary nonlinear dynamics techniques, namely the Lagrangian descriptor and the escape times. We initially consider the system with one and a half degrees of freedom and construct the PS. Then we calculate the Lagrangian descriptor for the system, but it is not possible to determine which structures of the phase space have stable and unstable behavior only by analyzing the LD. Therefore, to complement the analysis we calculate the escape times of the initial conditions. We show that the LD and the escape times faithfully reproduce the dynamics observed through the PS. Then, we introduce one more degree of freedom, the rotation, to the system, and through the LD and the ET techniques we study the dynamics of the forced Morse potential with rotation. We observe the existence of islandlike structures in which the escape times of the initial conditions are smaller in relation to their neighborhood, and we call them "escape islands." We could also visualize the stickiness around stable islands. Furthermore, we note that the introduction of rotation modifies the structure of the phase space, changing the position and the number of the equilibrium points. In particular, we have verified that for high-field amplitudes, the rotation leads to an increase of the stability region, which in turn should lead to a decrease of the photodissociation probability. This result is in agreement with previous quantum and semiclassical investigations of polar diatomic molecule dissociation under chirped pulses [36,37]. Physically, the decreasing of the dissociation probability with the inclusion of rotation can be attributed to the addition of the new degree of freedom: the energy pumped by the laser field can now also be distributed to the rotational modes, instead of being delivered exclusively to the vibrational motion. This behavior influences the probabilities of photodissociation, photoassociation; and the initial escape conditions [38–41]. Thus, we will use the LD

and ET to study the behavior of these probabilities in future work.

ACKNOWLEDGMENTS

We acknowledge support from the Brazilian scientific agency CAPES–Coordination for the Improvement of Higher Education Personnel. R.E.C. and E.F.L. gratefully acknowledge the support of FAPESP-São Paulo Research Foundation through Grants No. 2019/07329-4 and No. 2014/23648-9, respectively. E.F.L. also gratefully acknowledges the support of CNPQ-National Council for Scientific and Technological Development through Grant No. 423982/2018-4.

[1] M. Bitter and V. Milner, Experimental Demonstration of Coherent Control in Quantum Chaotic Systems, Phys. Rev. Lett. **118**, 034101 (2017).

[2] B. Pokharel, M. Z. R. Misplon, W. Lynn, P. Duggins, K. Hallman, D. Anderson, A. Kapulkin, and A. K. Pattanayak, Chaos and dynamical complexity in the quantum to classical transition, Sci. Rep. **8**, 2108 (2018).

[3] A. Lopez-Pina, J. C. Losada, R. M. Benito, and F. Borondo, Frequency analysis of the laser driven nonlinear dynamics of HCN, J. Chem. Phys. **145**, 0 (2016).

[4] G. E. Murgida, F. J. Arranz, and F. Borondo, Quantum control of isomerization by robust navigation in the energy spectrum, J. Chem. Phys. **143**, 214305 (2015).

[5] C. Chandre, J. Mahecha, and J. P. Salas, Driving the formation of the RbCs dimer by a laser pulse: A nonlinear-dynamics approach, Phys. Rev. A **95**, 033424 (2017).

[6] M. E. Goggin and P. W. Milonni, Driven Morse oscillator: Classical chaos, quantum theory, and photodissociation, Phys. Rev. A **37**, 796 (1988).

[7] D. W. Noid and J. R. Stine, Classical treatment of the dissociation of hydrogen fluoride with one and two infrared lasers, Opt. Commun. **31**, 161 (1979).

[8] R. B. Walker and R. K. Preston, Quantum versus classical dynamics in the treatment of multiple photon excitation of the anharmonic oscillator, J. Chem. Phys. **67**, 2017 (1977).

[9] N. Bloembergen, Comments on the dissociation of polyatomic molecules by intense 10.6 μm radiation, Opt. Commun. **15**, 416 (1975).

[10] K. M. Chrlstoffel and J. M. Bowman, Classical trajectory studies of multiphoton and overtone absorption of HF, J. Phys. Chem. **85**, 2159 (1981).

[11] Z.-M. Lu, M. Vallières, J.-M. Yuan, and J. F. Heagy, Controlling chaotic scattering: Impulsively driven Morse potential, Phys. Rev. A **45**, 5512 (1992).

[12] D. W. Noid and J. R. Stine, Infrared multiphoton dissociation with one and two lasers, Chem. Phys. Lett. **65**, 153 (1979).

[13] P. G. Drazin, *Nonlinear System* (Cambridge University Press, Cambridge, 1992).

[14] J. A. Jiménez-Madrid and A. M. Mancho, Distinguished trajectories in time dependent vector fields, Chaos **19**, 013111 (2009).

[15] F. Balibrea-Iniesta, C. Lopesino, S. Wiggins, and A. M. Mancho, Chaotic dynamics in nonautonomous maps: Application to the nonautonomous Hénon map, Int. J. Bifurcat. Chaos **25**, 1550172 (2015).

[16] C. Lopesino, F. Balibrea-Iniesta, S. Wiggins, and A. M. Mancho, Lagrangian descriptors for two-dimensional, area preserving, autonomous and nonautonomous maps, Commun. Nonlin. Sci. Num. Simul. **27**, 40 (2015).

[17] C. Lopesino, F. Balibrea-Iniesta, S. Wiggins, and A. M. Mancho, The chaotic saddle in the Lozi map, autonomous and nonautonomous versions, Int. J. Bifurcat. Chaos **25**, 1550184 (2015).

[18] F. Balibrea-Iniesta, C. Lopesino, S. Wiggins, and A. M. Mancho, Lagrangian descriptors for stochastic differential equations: A tool for revealing the phase portrait of stochastic dynamical systems, Int. J. Bifurcat. Chaos **26**, 1630036 (2016).

[19] M. Feldmaier, A. Junginger, J. Main, G. Wunner, and R. Hernandez, Obtaining time-dependent multi-dimensional dividing surfaces using Lagrangian descriptors, Chem. Phys. Lett. **687**, 194 (2017).

[20] T. Uzer, C. Jaffé, J. Palacián, P. Yanguas, and S. Wiggins, The geometry of reaction dynamics, Nonlinearity **15**, 957 (2002).

[21] F. Revuelta, F. R. M. Benito, and F. Borondo, Identification of the invariant manifolds of the LiCN molecule using Lagrangian descriptors, Phys. Rev. E **104**, 044210 (2021).

[22] V. J. García-Garrido and S. Wiggins, Lagrangian descriptors and the action integral of classical mechanics, Phys. D: Nonlin. Phenom. **434**, 133206 (2022).

[23] J. Montes, F. Revuelta, and F. Borondo, Lagrangian descriptors and regular motion, Commun. Nonlin. Sci. Num. Simul. **102**, 105860 (2021).

[24] G. G. Carlo and F. Borondo, Lagrangian descriptors for open maps, Phys. Rev. E **101**, 022208 (2020).

[25] Y. Gu and J.-M. Yuan, Classical dynamics and resonance structures in laser-induced dissociation of a Morse oscillator, Phys. Rev. A **36**, 3788 (1987).

[26] J. Heagy and J. M. Yuan, Dynamics of an impulsively driven Morse oscillator, Phys. Rev. A **41**, 571 (1990).

[27] G. Gopakumar, M. Abe, M. Kajita, and M. Hada, Ab initio study of permanent electric dipole moment and radiative lifetimes of alkaline-earth-metal–Li molecules, Phys. Rev. A **84**, 062514 (2011).

[28] R. Guérout, M. Aymar, and O. Dulieu, Ground state of the polar alkali-metal-atom–strontium molecules: Potential energy curve and permanent dipole moment, Phys. Rev. A **82**, 042508 (2010).

[29] M. A. Buldakov, V. N. Cherepanov, E. V. Koryukina, and Y. N. Kalugina, On some aspects of changing the sign of the dipole moment functions of diatomic molecules, J. Phys. B **42**, 105102 (2009).

[30] M. A. Buldakov and V. N. Cherepanov, The semiempirical dipole moment functions of the molecules HX (X = F, Cl, Br, I, O), CO and NO, J. Phys. B **37**, 3973 (2004).

[31] E. F. de Lima and R. Egydio de Carvalho, Effects of oscillatory behavior of the dipole function on the dissociation dynamics of the classical driven Morse oscillator, Physica D **241**, 1753 (2012).

[32] A. M. Mancho, S. Wiggins, J. Curbelo, and C. Mendoza, Lagrangian descriptors: A method for revealing phase space structures of general time dependent dynamical systems, Commun. Nonlin. Sci. Num. Simul. **18**, 3530 (2013).

[33] G. Haller, Lagrangian coherent structures, Ann. Rev. Fluid. Mech. **47**, 137 (2015).

[34] C. Lopesino, F. Balibrea-Iniesta, V. García-Garrido, S. Wiggins, and A. M. Mancho, A theoretical framework for Lagrangian descriptors, Int. J. Bifurcat. Chaos **27**, 1730001 (2017).

[35] F. Revuelta, R. M. Benito, and F. Borondo, Unveiling the chaotic structure in phase space of molecular systems using Lagrangian descriptors, Phys. Rev. E **99**, 032221 (2019).

[36] S. Chelkowski and A. D. Bandrauk, Control of molecular vibrational excitation and dissociation by chirped intense infrared laser pulses. Rotational effects, J. Chem. Phys. **99**, 4279 (1993).

[37] J.-H. Kim, W.-K. Liu, F. R. W. McCourt, and J.-M. Yuan, Dissociation of diatomic molecules by elliptically polarized chirped pulses, J. Chem. Phys. **112**, 1757 (2000).

[38] M. D. Forlevesi, R. Egydio de Carvalho, and E. F. de Lima, A tunable mechanism to control photo-dissociation with invariant tori with variable energies, Phys. A **490**, 681 (2018).

[39] E. F. de Lima, R. E. Egydio de Carvalho, and M. D. Forlevesi, Nonchaotic laser pulse dissociation through deformed tori, Phys. Rev. E **101**, 022207 (2020).

[40] A. K. de Almeida Jr., R. Egydio de Carvalho, and E. F. de Lima, Controlling dissociation by trapping trajectories in highly energetic states, Phys. A **449**, 101 (2016).

[41] M. D. Forlevesi, R. E. Egydio de Carvalho, and E. F. de Lima, Nonlinear photoassociation through exotic orbits, Phys. Rev. E **104**, 014206 (2021).